Identification of Tree Species and Extent of Material Deterioration of Wood Components in the Yangjia Courtyard Ancient Building

Yan Yang Bin Li Yuqing Liu Wenqiang Zhang
Chuanbo Wang

Abstract

The identification of the tree species and the extent of material deterioration in the wooden components of the walkway of the first courtyard of the ancient Yangjia Courtyard were analyzed in this study using bright-field microscopy, polarized light, fluorescence, and Fourier-transform infrared (FTIR) spectroscopy methods. The results are as follows: (1) samples No. 1 and No. 2, and No. 4, No. 3, and No. 5 taken from the roots of the wooden pillars were identified as lace-bark pine wood (*Pinus bungeana*), poplar woods (*Populus* spp.), large-fruited elm wood (*Ulmus macrocarpa*), and spruce wood (*Picea* sp.), respectively on the basis of observation of anatomical structural characteristics and analysis of selection principle of ''local selection'' in ancient buildings. (2) The observation of polarization and fluorescence and the analysis of FTIR spectra showed that the brightness of crystalline cellulose birefringence reduced severely, and analysis of FTIR spectra showed that the absorption peaks representing cellulose and hemicellulose in the lace-bark pine and spruce wooden components disappeared or decreased. However, the polarization and fluorescence and the FTIR spectra of the poplar and elm wooden components showed that the brightness of the crystalline cellulose birefringence and the absorption peaks remained constant, as the controls did. (3) According to the results of the effects of the polarization and fluorescence effects and the FTIR spectra, we concluded that the lace-bark pine and spruce wooden components were severely attacked by brown rot fungi; in contrast, the wooden components of poplar and elm were not attacked by wood decay fungus, but were attacked by insects. These results provide scientific guidance for subsequent preventive conservation such as preservative treatment and insect prevention.

The former residence of Yang Tingbao, a well-known architect and educationalist, was built originally during the Qing Dynasty. It is located on Jiefang Road, Wancheng District, Nanyang City, Henan Province, China. It covers an area of more than 10,000 m^2 and includes the Yang Family Courtyard, the Xu Family Courtyard, and the Taigu Car Sugar Company. Originally there were seven courtyards, but only five remain today. Currently it is the most complete and largest residential architecture found in Nanyang and is a typical example of residential architecture in southwestern Henan Province. It contains rich folk-culture connotations, reflecting the life, living conditions, and folk customs of the local people of southwestern Henan Province during the late Qing Dynasty and the Republic of China. It is an essential piece of first-hand information for the study of Nanyang's residential architecture during the Ming and Qing dynasties, the history of modern China and modern Chinese architecture, and Nanyang's folk culture. It was declared a municipal key cultural relic protection unit in Nanyang City in 2002 and a provincial key cultural relic protection unit in Henan Province in 2006 for its high historical, scientific, cultural, and other values.

Nevertheless, some wooden components, particularly the roots of wooden pillars (Figs. 1c through 1g), have been degraded to different degrees. It is well known that degradation behavior inevitably leads to changes of anatomical structures (Bari et al. 2019, 2020; Diandari et al. 2020; Yang et al. 2021a, 2022a, 2022b, 2022c) and degradation of chemical components (Tamburini et al. 2017;

The authors are, respectively, Associate Professor, Associate Professor, Undergraduate, Undergraduate, and Undergraduate, School of Architecture, Nanyang Inst. of Technol., Nanyang City, Henan Province, China (yangyanrainy@163.com [corresponding author], 165400683@qq.com, 785698416@qq.com, 2066645117@qq.com, and 785698416@qq.com). This paper was received for publication in November 2022. Article no. 22-00068.

Forest Prod. J. 73(2):82–93.
doi:10.13073/FPJ-D-22-00068

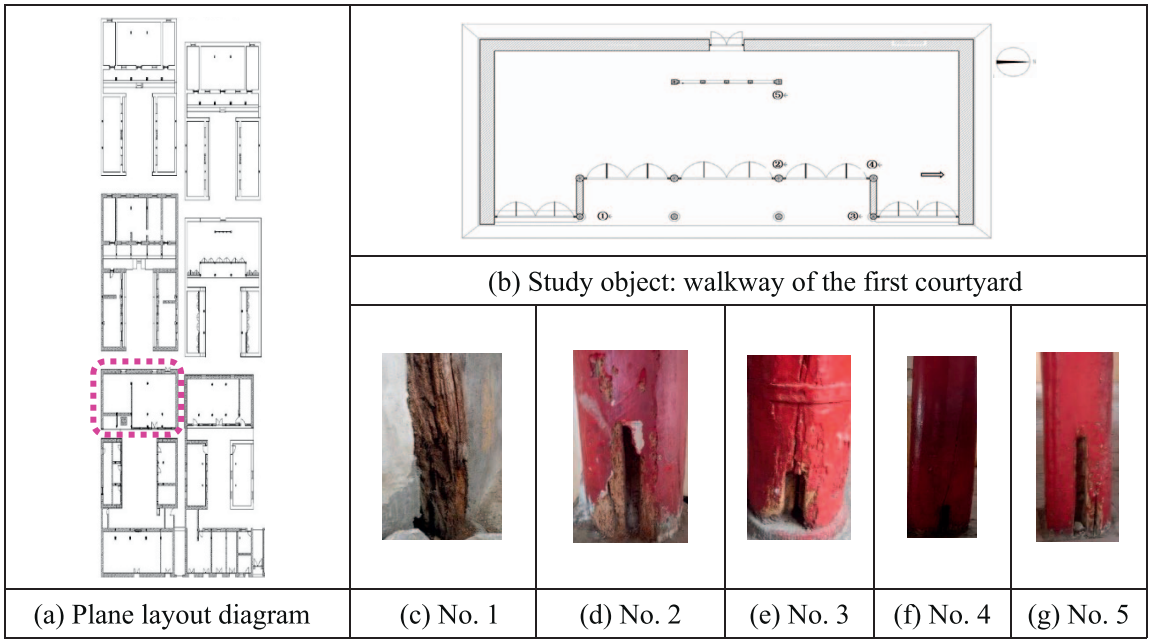

Figure 1.—Plane layout diagram and materials.

Sun et al. 2020b; Yang et al. 2020a, 2021b, 2022b, 2022c). The changes of the anatomical structures and the chemical components eventually will decrease the mechanical strength of wooden components (Ueda et al. 2020) and affect the safety and the life span of ancient buildings.

In general, the distribution and the content of cellulose crystalline regions and lignin in the cell walls of wood can be determined qualitatively using polarized light and fluorescence, respectively. The higher the birefringence brightness of crystalline cellulose, the higher the relative content of cellulose; accordingly, the greater the brightness of fluorescence intensity, the higher the relative content of lignin (Kanbayashi and Miyafuji 2016; Kiyoto et al. 2018; Yang et al. 2021a, 2022a, 2022b, 2022c). In addition, because of the main chemical compositions of wood having corresponding characteristic infrared absorption spectra, the shapes, positions, and intensities of the absorption peaks in Fourier-transform infrared (FTIR) spectra will be modified, accompanied by the shift of chemical components of wood (Liu et al. 2017; Tamburini et al. 2017; Croitoru et al. 2018; Fahey et al. 2019; Wentzel et al. 2019; Bari et al. 2020; Dong et al. 2020; Yang et al. 2020a, 2021b, 2022b). Therefore, the changes in the functional groups and the content of the main chemical component can be determined from the changes in the intensity of the absorption peaks in the FTIR characteristic spectra.

On the basis of the protective principle of minimum intervention for ancient buildings, the methods of polarized light, fluorescence (Yang et al. 2021a, 2022a, 2022b, 2022c), FTIR (Yang et al. 2020a, 2021b, 2022b), X-ray diffraction (Broda and Popescu 2019, Broda et al. 2022, Yang et al. 2022c), and so on are used to evaluate the extent of decay of wooden components because of the advantages of requiring a minimal number of samples, resulting in less damage to ancient buildings compared with conventional gravimetric techniques.

The goal of the present study is to obtain the cause of the decay by identifying the tree species, and to obtain the extent of decay of the wooden components in Yangjia Courtyard ancient building using polarized light, fluorescence, and FTIR methods. Such a study of the extent of decay will provide scientific data for future conservation and restoration of the ancient buildings in Yang's former residence.

Materials and Methods

Materials

Samples were collected from the roots of the wooden components in walkway of the first courtyard of Yangjia Courtyard ancient building (Figs. 1a and 1b) and were adopted with an increment borer (10–100–1027, Haglöf AB, Mora, Sweden). Sample No. 1 was decayed seriously (Fig. 1c), whereas samples Nos. 2, 3, 4, and 5 were gnawed severely by insects, as observed (Figs. 1d, 1e, 1f, and 1g). The control samples were obtained from the healthy locations in these wooden components.

Methods

Treatment and preparation of samples.—The embedding treatment with polyethylene glycol (molecular weight 2,000) and the sectioning of the samples with a microtome (HistoCore AUTOCUT, Leica Biosystems, Nussloch, Germany) for identification of tree species, observations of polarized light, and fluorescence were performed according to previous papers (GB/T29894-2013; Yang et al. 2021a, 2022a, 2022b, 2022c). Preparation for FTIR analysis also followed the methods of other studies (Yang et al. 2020a, 2021b, 2022b).

Identification of tree species.—Anatomical structures of the samples were observed by a biological digital microscope (ECLIPSE Ni-U, Nikon, Tokyo, Japan), whereas anatomical features were described according to the International Association of Wood Anatomists (IAWA) list of microscopic features for hardwood identification (Wheeler et al. 1989), IAWA list of microscopic features for

softwood identification (Richter et al. 2004) and Chinese Timber Records (Cheng et al. 1992).

Observation of polarized light and fluorescence.—The analysis of polarization and fluorescence effects was observed by a fluorescence microscope (ECLIPSE Ni-U, Nikon). The distribution and content of cellulose and lignin were analyzed under polarized light and fluorescence (blue-light excitation and green-light excitation) for the analysis of decay extent of the wooden components, respectively (Yang et al. 2021a, 2022a, 2022b, 2022c). Five slices were made for each sample, and 5 to 10 pictures were randomly taken for each slice.

FTIR testing.—FTIR testing was conducted using a FTIR spectrophotometer (ALPHA2, Bruker, Billerica, MA) at a range of 4,000 cm^{-1} to 400 cm^{-1} to provide detailed information on the functional groups present in the sample surface. The scans were run at a resolution of 4 cm^{-1} and the spectra were obtained using attenuated total reflectivity (Bari et al. 2020; Dong et al. 2020; Yang et al. 2020a, 2021b, 2022b). A minimum of five scans per specimen was done.

Results and Discussion

Anatomical structural characteristics and identification of tree species

Figure 2 shows the microstructure of sample No 1. The growth rings are characterized by a gradual transition from earlywood and latewood (Fig. 2a). Thus, the earlywood is characterized by square, rectangular, and polygonal tracheids with thin-walled cells (Fig. 2b), whereas the latewood is composed of rectangular and square tracheids with thick-walled cells (Fig. 2c). The bordered pittings in radial walls of the earlywood tracheids are uniseriate (Fig. 2d). No helical thickenings are observed on tracheids (Figs. 2d and 2e). The axial parenchymas are absent in the transverse section (Figs. 2a through 2c). The rays are of two types: one is single row and the other is spindle shaped; the height of a single row of rays is 3 to 8 cells, whereas spindle-shaped rays are 2 to 3 cells wide and 3 to 12 cells high (Fig. 2f). The ray cells include the ray tracheids and the ray parenchyma cells. Ray tracheids are located at the upper and lower ends of the ray parenchyma cells. Occasionally, the low rays are composed of obvious dentate ray tracheids (Figs. 2d and 2e). The horizontal wall of ray cells with more pittings is thick, whereas there are obvious nodules in the end wall (Fig. 2e). The radial section also shows the classic features: pinoid cross-field pittings in the cross-field between ray parenchyma cells and earlywood axial tracheids (Fig. 2d). The intercellular canals contain both axial and radial canals. The axial canals are mostly single and normally distribute in the latewood and the nearby earlywood seen from transverse section (Figs. 2a and 2c); the radial canals locate in the spindle-shaped wood rays seen from tangential section (Fig. 2f). On the basis of the observation of anatomical structural characteristics, it can be concluded that sample No. 1 is lace-bark pine wood (*Pinus bungeana*, Pinaceae; Cheng et al. 1992).

Figures 3 and 4 show the microstructures of samples from Nos. 2 and 4, respectively. The distribution of the vessels that are orbicular-ovate and elliptical-circular in the transverse section is diffuse-porous wood or semiring-porous, whereas the arrangement of the vessels is radial; furthermore, the combination of vessels is mainly radial multiples of two to four cells and a few of solitary (Figs. 3a and 4a); no tyloses or gums were found in the vessels; also no helical thickenings of vessels were found throughout the body of vessel elements (Figs. 3b and 4b). The type of perforation is simple perforation plate and that of intervessel pittings is alternate (Figs. 3b and 4b). A few marginal and diffuse-in-aggregates axial parenchymas were found (Figs. 3a and 4a). The cell walls of wood fibers with distinctly

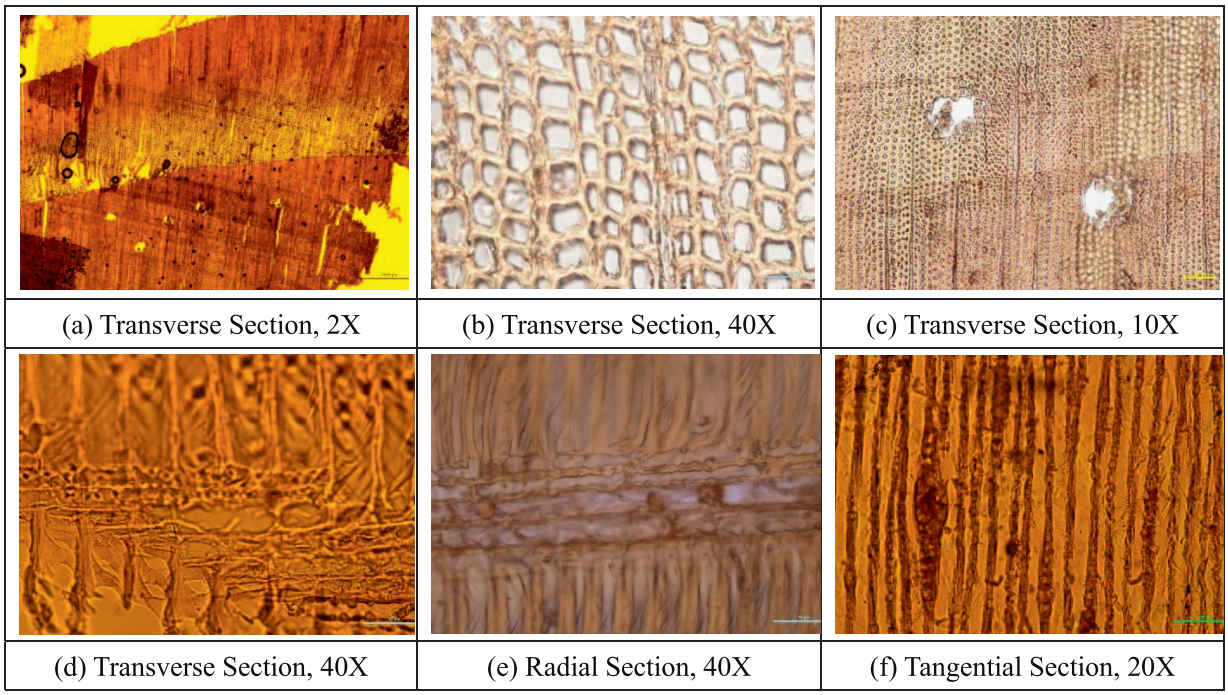

Figure 2.—Microstructures of sample No. 1 under bright-field microscope.

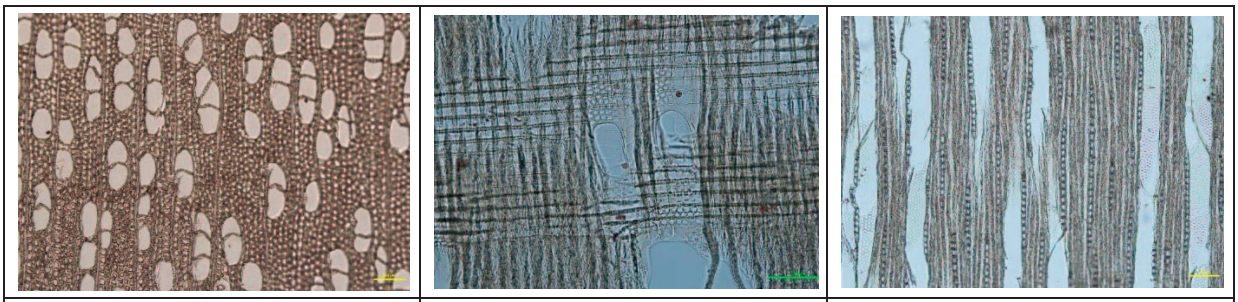

(a) Transverse Section, 10X	(b) Radial Section, 20X	(c) Tangential Section, 10X

Figure 3.—Microstructures of sample No. 2 under bright-field microscope.

(a) Transverse Section, 10X	(b) Radial Section, 20X	(c) Tangential Section, 10X

Figure 4.—Microstructures of sample No. 4 under bright-field microscope.

simple pittings are thin. All ray cells are procumbent and one cell wide (Figs. 3c and 4c). No axial or radial intercellular canals were found in these woods (Figs. 3a and 3c and Figs. 4a and 4c). On the basis of the microstructure observations, it can be concluded that samples Nos. 2 and 4 are poplar woods (*Populus* spp., Salicaceae; Cheng et al. 1992).

Figure 5 shows the microstructures of sample No. 3. As shown, the distribution of vessels is ring-porous wood; the vessels in the earlywoods one to three cells wide are circular, oval-circle, and orbicular-ovate on the transverse section (Fig. 5a); the arrangement of vessels in latewood is tangential wary bands, and the combinations are mainly clusters common, with a few exclusively solitary and radial multiples (Fig. 5a). The type of perforations is simple perforation plate, whereas the type of intervessel pits is alternate (Fig. 5a); helical thickening of vessels was found throughout the body of vessel elements. Many paratracheal axial parenchymas were found: vasicentric, diffuse in aggregates, and wavy banded parenchyma that are more than three cells wide (Fig. 5a). Wood rays were two to six cells wide; all ray cells are procumbent cells, and no special cells were found in ray cells (Figs. 5b and 5c). Moreover, no axial or radial intercellular canals were found (Figs. 5a and 5c). On the basis of the microstructure observations, it can be concluded that sample No. 3 is elm wood (*Ulmus* sp., Ulmaceae; Cheng et al. 1992).

Figure 6 shows the microstructure of sample No. 5. The growth rings are characterized by a gradual transition from earlywood to latewood (Fig. 6a). Thus, the earlywood is characterized by square, rectangular, and polygonal tracheids with thin-walled cells (Fig. 6b), whereas the latewood is composed of rectangular and square tracheids with thick-walled cells (Fig. 6c). The bordered pittings in

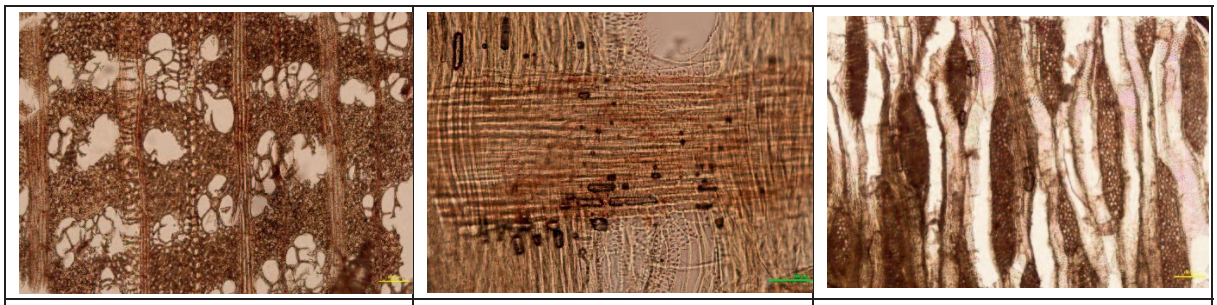

(a) Transverse Section, 4X	(b) Radial Section, 20X	(c) Tangential Section, 10X

Figure 5.—Microstructures of sample No. 3 under bright-field microscope.

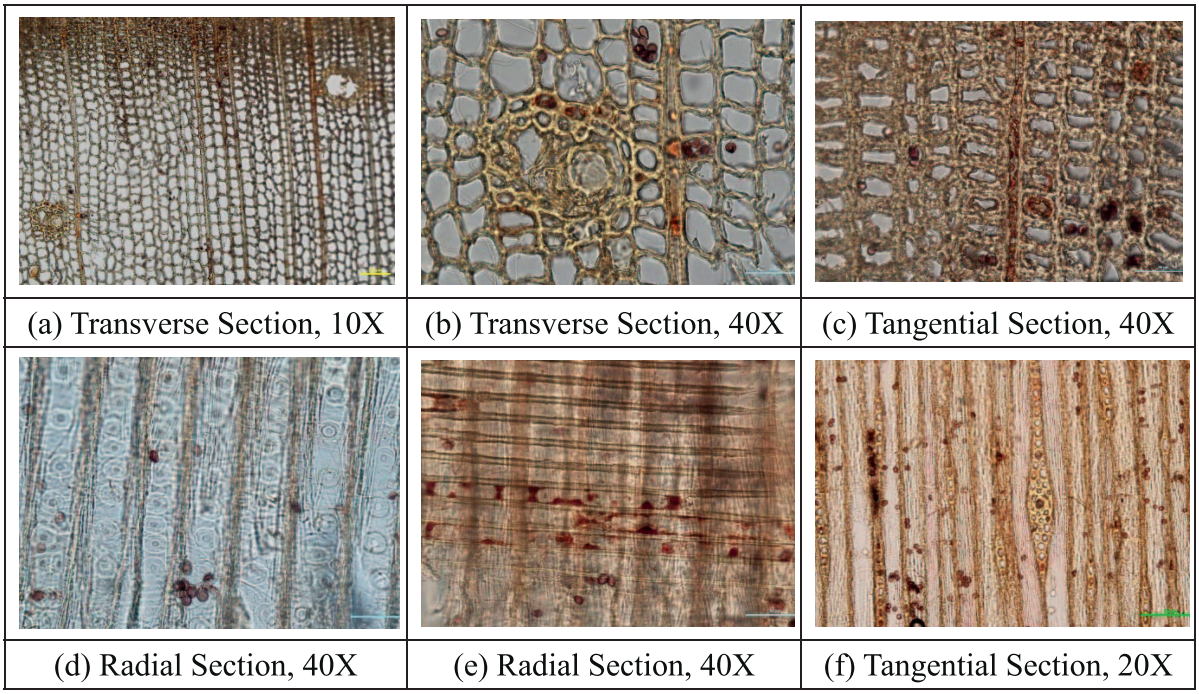

Figure 6.—Microstructures of sample No. 5 under bright-field microscope.

radial walls of the earlywood tracheids are uniseriate (Fig. 6d). Helical thickenings are shown in parts of tracheids (Fig. 6d). The axial parenchymas are absent in the transverse sections (Figs. 6a through 6c). The rays are of two types: one is single row and the other is spindle shaped, the height of a single row of rays is 3 to 12 cells, whereas spindle-shaped rays are 2 to 3 cells wide and 3 to 12 cells high (Fig. 6f). The ray cells include the ray tracheids and the ray parenchyma cells. Ray tracheids are located at the upper and lower ends of the ray parenchyma cells. Occasionally, the low rays are composed of obvious dentate ray tracheids (Fig. 6e). The horizontal wall of ray cells with more pittings is thick, whereas there are obvious nodules in the end wall (Fig. 6e). The radial section also shows the classic features: piceoid cross-field pittings in the cross-field between ray parenchyma cells and earlywood axial tracheids (Fig. 6e). The intercellular canals contain both axial and radial canals. The axial canals are mostly single and the walls of secreting fatty cells are thick (Fig. 6b), whereas the radial canals locate in the spindle-shaped wood rays and are smaller than axial canals (Fig. 6f). On the basis of observation of anatomical structural characteristics, it can be concluded that sample No. 5 is spruce wood (*Picea* sp., Pinaceae; Cheng et al. 1992).

Analysis of the effect of polarization and fluorescence

Figure 7 shows the effect of polarization and fluorescence on the lace-bark pine wooden component. The birefringence brightness of crystalline cellulose shows unobviously in the cell walls of the earlywood tracheids under polarized light (Fig. 7a) compared with the control sample (Fig. 7g). Though the birefringence brightness of crystalline cellulose shows obviously in the cell wall corners (CC) and the compound middle lamellas (CML) of the latewood tracheids, it is almost lacking in the middle layers (S_2) and the inner layers (S_3) of the secondary wall (S) (Fig. 7d) compared with the control sample (Fig. 7j). The brightness of green and red fluorescence of lignin shows obviously in the cell walls of the earlywood (Figs. 7b and 7c) and latewood (Figs. 7e and 7f) tracheids under fluorescent light and is nearly consistent with that in the control samples (Figs. 7h and 7i [earlywood] and 7k and 7l [latewood]). From the effect of polarization, both of green and red fluorescence, it can be concluded that the content of cellulose in the lace-bark pine wooden component decreased a great deal, whereas lignin remained abundant in tracheids, after comparison with the control sample.

Figures 8 and 9 show the effect of polarization and fluorescence on the poplar and elm wooden components, respectively. Under polarized light (Figs. 8a and 8d and Figs. 9a and 9d), the birefringence brightness of crystalline cellulose in the cell walls of the vessels and wood fibers is apparently observed and is consistent with the control samples (Figs. 8g and 9g), indicating that cellulose remains in these cell walls. Under fluorescent light (Figs. 8b, 8c, 8e, and 8f and Figs. 9b, 9c, 9e, and 9f), the brightness of the green and red fluorescence of lignin in the cell walls of the vessels and wood fibers is also evident compared with the control samples (Figs. 8h and 8i and Figs. 9h and 9i), indicating that an abundance of lignin exists in the cell walls of the vessels and wood fibers. From these observations, we conclude that cellulose and lignin were not consumed by decay fungi but that they were severely attacked by insects. The result is consistent with that in our previous study of the poplar and elm wooden components in the Danxia Temple ancient building (Yang et al. 2021a).

Figure 10 shows the effect of polarization and fluorescence on the spruce wooden component. The birefringence brightness of crystalline cellulose shows unobviously in the cell walls of the earlywood tracheids under polarized light (Fig. 10a) compared with the control sample (Fig. 10d).

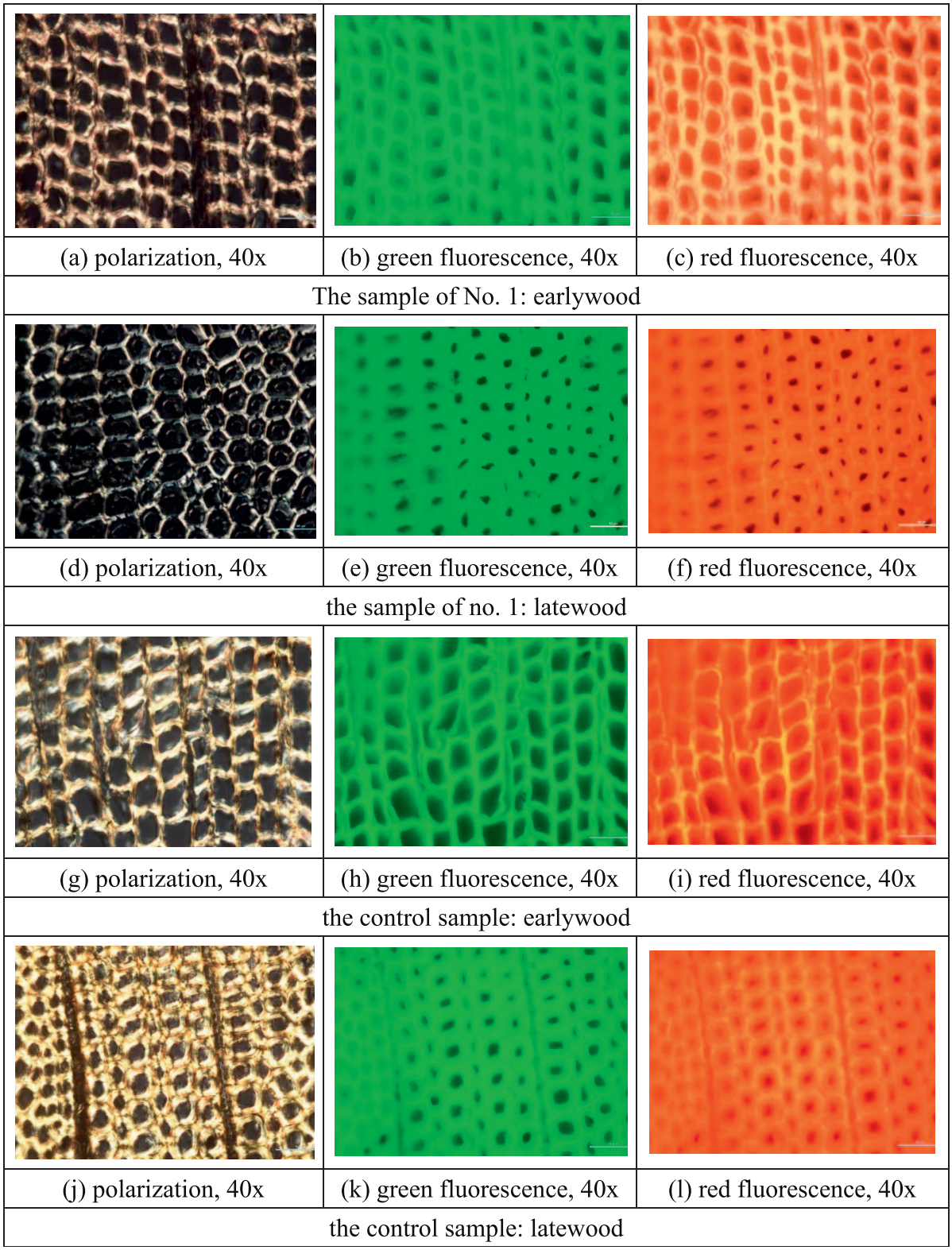

*Figure 7.—Effects of polarization and fluorescence on lace-bark pine woods (*Pinus bungeana*) in transverse sections.*

However, the birefringence brightness of crystalline cellulose shows obviously in the CC and CML of the latewood tracheids; this is almost lacking in the S2 and S3 layers of the secondary wall (Fig. 10b) compared with the control sample (Fig. 10j). The brightness of green and red fluorescence of lignin in the cell walls shows obviously both in the earlywood (Figs. 10 and 10c) and latewood (Figs. 10e and 10f) tracheids and are nearly consistent with that in the control sample (Figs. 10h and 10i [earlywood] and 10k and 10l [latewood]). From the effect of polarization

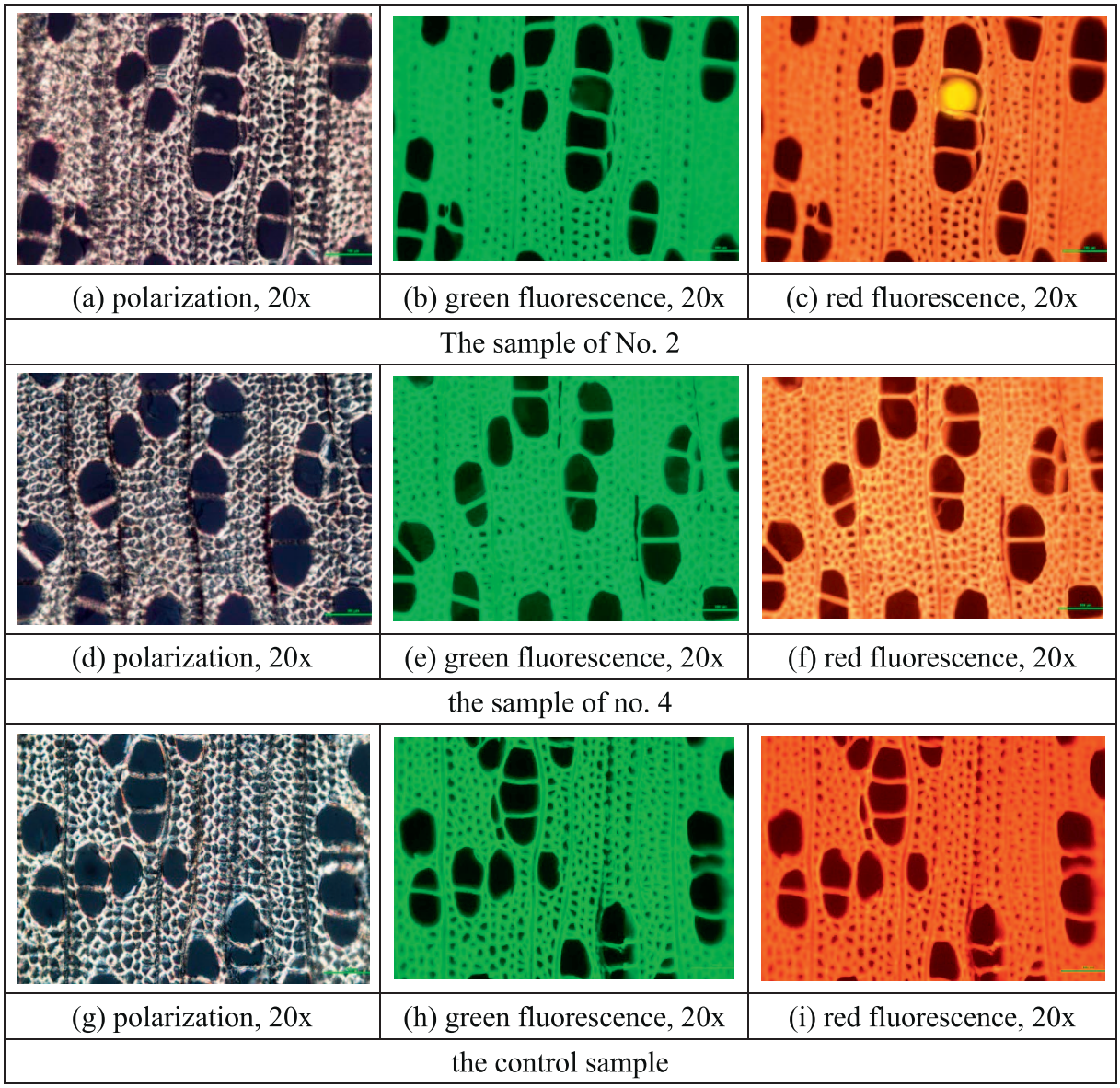

*Figure 8.—Effect of polarization and fluorescence on poplar wooden components (*Populus *spp.) in transverse sections.*

and green and red fluorescence, it can be concluded that the content of cellulose in the spruce wooden component decreased a great deal, whereas lignin remained abundant in tracheids of the spruce wooden component.

From these observations of the effect of polarization and fluorescence (Figs. 7 through 10), it can be concluded that the cellulose of the lace-bark pine and spruce wooden components was severely attacked by brown rot fungi, which consume only cellulose and hemicellulose but leave lignin (Guo et al. 2010). The poplar and elm wooden components were not attacked by wood decay fungi but by insects.

FTIR analysis of the decayed wooden components

As can be seen from Figs. 11 through 14, the positions of the absorption peaks of the wooden components in the region from 1,800 to 800 cm^{-1} have no displacement, but the intensities have obvious changes.

In contrast to the control sample of the lace-bark pine wood, the absorption peaks at 1,735 cm^{-1} for the unconjugated C=O in xylans in hemicellulose and 1,058 cm^{-1} for the C–O stretch in cellulose and hemicellulose disappear, as seen in Fig. 11. In addition, the intensities of the absorption peaks at 1,374 cm^{-1} for the C–H deformation in cellulose and hemicellulose, at 1,159 cm^{-1} representing C–O–C vibration in cellulose and hemicellulose, and at 897 cm^{-1} representing C–H deformation in cellulose show a large decrease, indicating that the cellulose and hemicellulose were severely degraded. However, the intensities of the absorption peaks at 1,649 cm^{-1} for the C=O stretching in the conjugated carbonyl group and at 1,598 cm^{-1} and 1,508 cm^{-1} for the aromatic skeleton representing lignin remain constant compared with the control sample; those at 1,460 cm^{-1} for C–H deformation in lignin, 1,424 cm^{-1} for C–H deformation in lignin, and 1,260 cm^{-1} for guaiacyl ring breathing, C–O stretch in lignin, and for C–O linkage in guaiacyl aromatic methoxyl groups show a large increase,

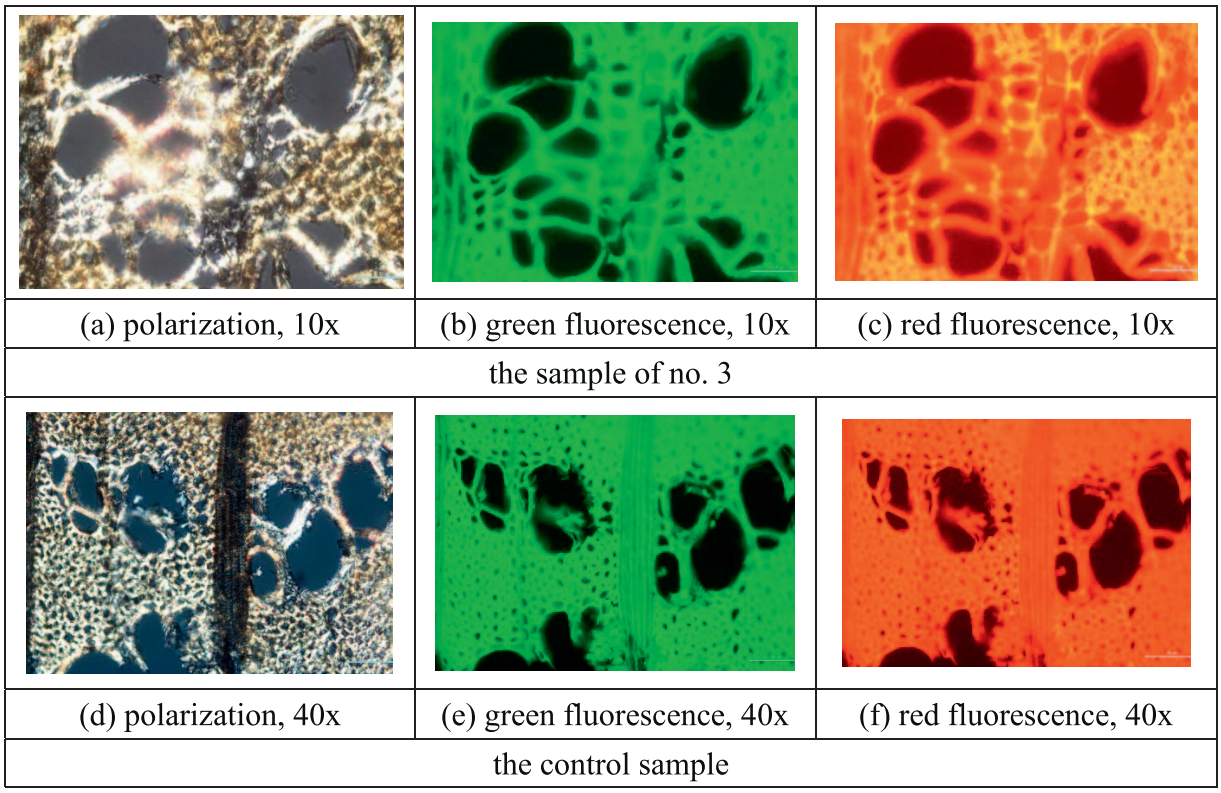

*Figure 9.—Effect of polarization and fluorescence on elm wooden components (*Ulmus *spp.) in transverse sections.*

indicating an increase in the relative content of lignin. From the FTIR analysis (Fig. 11), we conclude that lignin in the lace-bark pine wooden component was mainly retained, whereas both cellulose and hemicellulose were degraded by the decay fungi. The results of FTIR spectroscopy seen in Figure 11 are consistent with the effect of polarization and fluorescence seen in Figure 7, and further confirm that the lace-bark pine wooden component was attacked by the brown rot fungi.

In contrast to the control samples of poplar and elm woods, the intensities of the absorption peaks at 1,735 cm^{-1}, 1,374 cm^{-1}, 1,158 cm^{-1}, 1,058 cm^{-1}, and 897 cm^{-1} of the poplar and elm wooden components almost remain unchanged in sample Nos. 2, 3, and 4 in Figures 12 and 13; in addition, the intensities of the absorption peaks at 1,649 cm^{-1}, 1,508 cm^{-1}, 1,460 cm^{-1}, 1,424 cm^{-1}, and 1,260 cm^{-1} also remain constant. From the FTIR results, we conclude that though the poplar and elm wooden components were consumed by insects, the main chemical compositions of cellulose, hemicellulose, and lignin were not significantly damaged by wood decay fungi. The results of FTIR spectroscopy (Figs. 11 and 12) are consistent with the effect of polarization and fluorescence in the poplar and elm wooden components (Figs. 8 and 9).

This can be seen in Figure 14, where the absorption peaks at 1,735 cm^{-1} and 1,159 cm^{-1} of the spruce wooden component disappear compared with the control sample; in addition, the intensities of the absorption peaks at 1,374 cm^{-1} and 897 cm^{-1} remain constant, and that at 1,058 cm^{-1} decreases. Meanwhile, the intensities of the absorption peaks at 1,598 cm^{-1}, 1,508 cm^{-1}, 1,460 cm^{-1}, 1,424 cm^{-1}, and 1,260 cm^{-1} increase considerably compared with the control sample. From the results of FTIR spectroscopy, we conclude that both the cellulose and hemicellulose in the spruce wooden component were attacked by wood decay fungi, whereas lignin was predominantly preserved. The results are consistent with the effect of polarization and fluorescence (Fig. 10), and further confirm that the spruce wooden component was attacked by brown rot fungi and not by insects.

Discussion

From the observations of the effect of polarization and fluorescence and the analysis of FTIR spectra, it can be concluded that cellulose and hemicellulose of the lace-bark pine and spruce wooden components were severely attacked by brown rot fungi, whereas those of poplar and elm were not attacked by wood decay fungi but by insects.

On the basis of the selection principle of ‘‘local selection’’ in ancient buildings, it can be concluded that these woods, such as lace-bark pine wood (*P. bungeana*), abele (*Populus alba*), clear stream poplar (*Po. rotundifolia* var. *duclouxiana*), cathay poplar (*Po. cathayana*), white gourd poplar (*Po. purdomii*), and large-fruited elm (*Ulmus macrocarpa*) are widely distributed in western Henan Province, China (GB/T16734-1997; Cheng et al. 1992). There are numerous attractive characteristics in these woods, such as the straight grain, the delicate and uniformity of structure, and the minute dry shrinkage. However, they also have some drawbacks. The lace-bark pine and spruce woods have low air-dry density (approximately 0.40 to 0.45g/cm^3), low strength, and low toughness, especially low resistance to wood decay fungi (Cheng et al. 1992); they also have low pH values (the range of 4.0 to 5.5), showing a strong acidity (Liu and Zhao 2012).

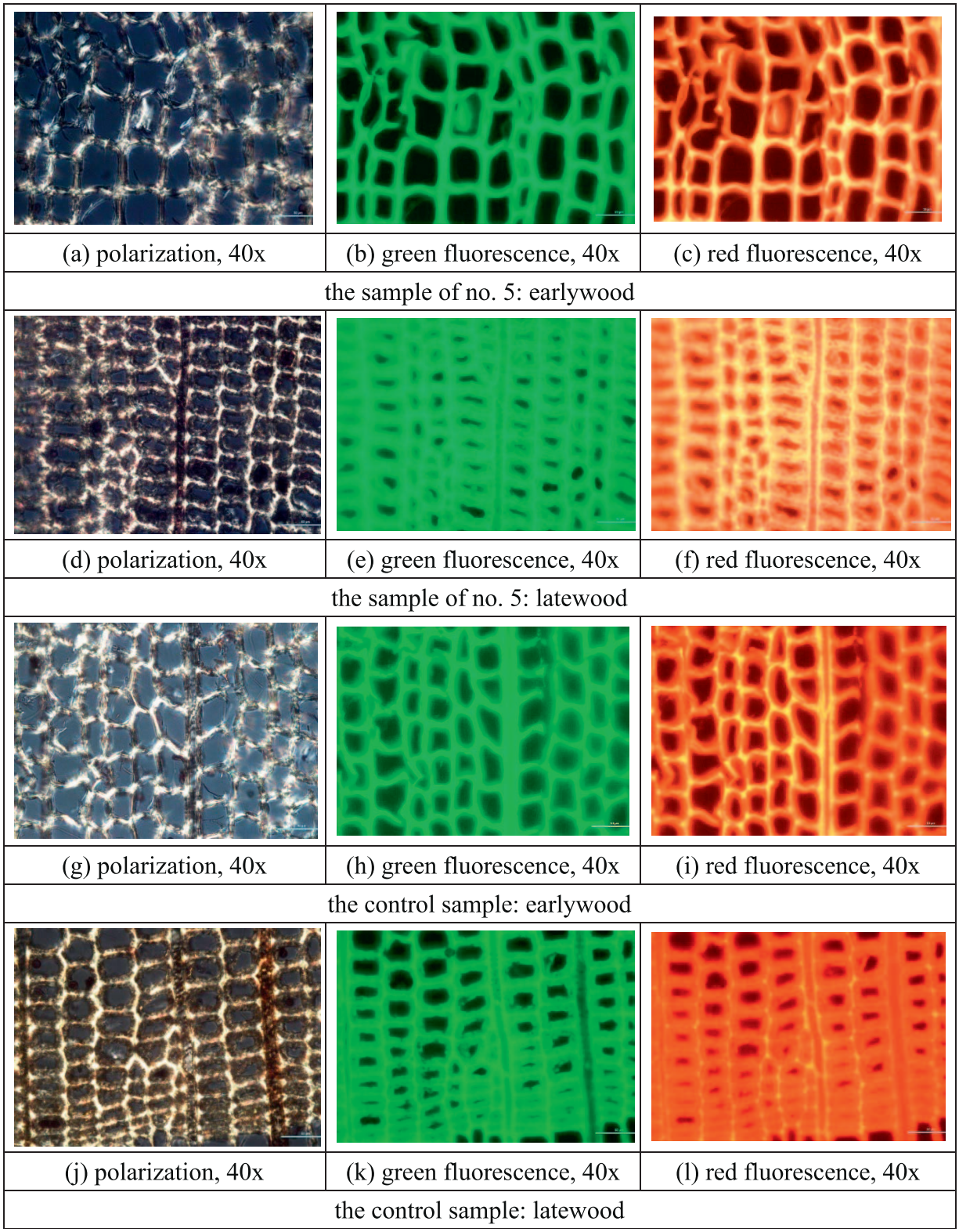

*Figure 10. Effect of polarization and fluorescence of spruce wooden components (*Picea *sp.) in transverse sections.*

As a rule, the decay of wood is the result of the activity of the wood decay fungi under suitable conditions such as abundant nutrients (rich carbon sources such as cellulose and hemicellulose, nitrogen sources, inorganic salts, and auxin and other chemical components, which provide indispensable nutrients for the growth of timber-decaying fungi.), adequate water (20% to 130% moisture content), suitable temperature (25°C to 40°C), acidic medium (4.0 to 6.5 pH), and adequate oxygen (1.5 mmHg to 10 mmHg; Guo et al. 2010). The low pH values of the lace-bark pine

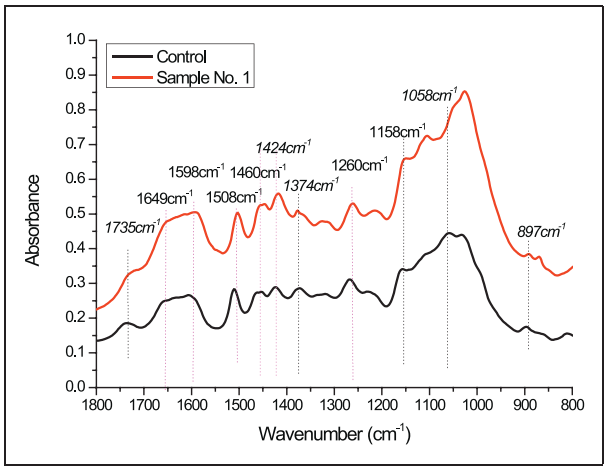

*Figure 11.—Fourier-transform infrared spectrum of lace-bark pine woods (*Pinus bungeana*).*

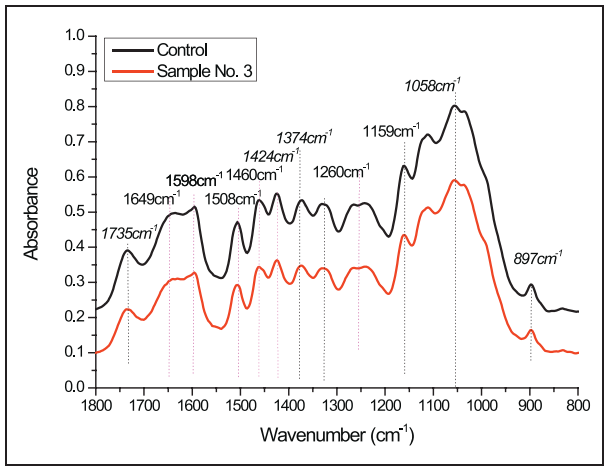

*Figure 13.—Fourier-transform infrared spectrum of elm wooden components (*Ulmus *spp.).*

and spruce wooden components provide an essential condition for the growth of wood decay fungi. This is an important reason why these two wooden components are susceptible to damage from decay fungi. Because of the protection of guaiacyl units, lignin has high decay resistance in coniferous woods; the brown rot fungi invade selectively the cellulose and hemicellulose, but leave the lignin (Guo et al. 2010). This is the reason why these lace-bark pine and spruce wooden components in this study were severely damaged by brown rot fungi during their long-term use. It is well known that cellulose plays a role in the skeleton of the cell wall; a reduction in cellulose content therefore results in a decrease in tensile strength, compressive strength, and other properties of the wooden components (Liu and Zhao 2012), ultimately affecting the longevity of ancient buildings.

In our previous research, we found that the poplar and elm woods were widely used on the wooden components in ancient buildings of Danxia Temple (Yang et al. 2021a). There are 62 species of poplar trees in China and they are mainly distributed in north China, NW China, and NE China (GB/T16734-1997; Cheng et al. 1992). As a whole, there is little difference in wood quality throughout the *Populus* genus, such as the straight grain, the delicate and uniformity of structure, and the minute dry shrinkage, low air-dry density (approximately 0.40 g/cm^3), low strength, and low toughness; in particular, they have a low resistance to termites (Cheng et al. 1992). The *Ulmus* genus is divided into two main groups: one is elm class (such as *U. castaneifolia*, *U. davidiana* var. *japonica*, *U. laciniata*, *U. macrocarpa*, *U. pumila*, etc.), with a dry-air density of 0.50 to 0.60 g/cm^3, and the other is *Ulmus parvifolia* class, with a dry-air density of 0.90 g/cm^3. The woods of the elm class are generally softer and less resistant to insects than those of the *Ulmus parvifolia* class (Cheng et al. 1992). In addition, the study of Liu and Zhao (2012) concluded that the pH values of the *Populus* spp. and *Ulmus* spp. woods are in the range of 7.0 to 9.3, indicating high alkalinity. This is an important reason why the poplar and elm wooden components in this study were not damaged by wood decay fungi during their long-term use.

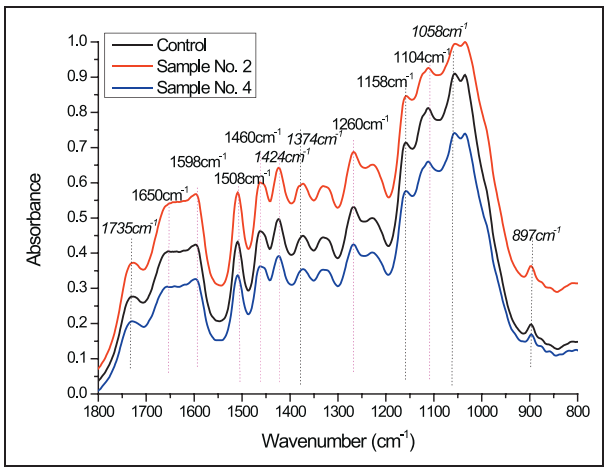

*Figure 12.—Fourier-transform infrared spectrum of poplar wooden components (*Populus *spp.).*

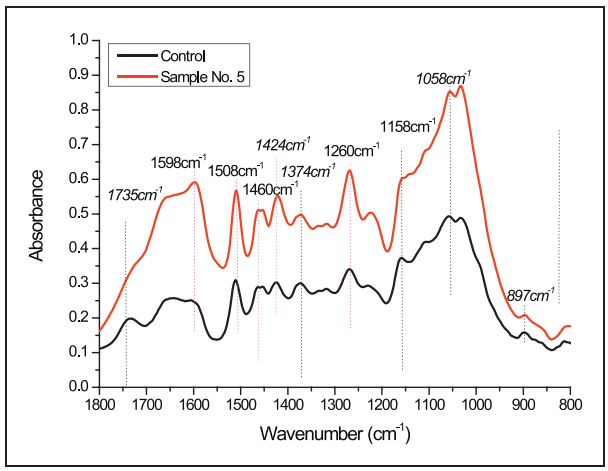

*Figure 14.—Fourier-transform infrared spectrum of spruce wooden components (*Picea *sp.).*

Conclusions

The identification of tree species was carried out using bright-field microscopy, and the extent of material deterioration in the wooden components of the ancient building of Yangjia Courtyard was observed and analyzed using polarized light, fluorescence, and FTIR methods.

1. On the basis of the observation of anatomical structural characteristics and the analysis of the selection principle of ''local selection'' in ancient buildings, it can be concluded that sample No. 1 is lace-bark pine wood (*Pinus bungeana*), samples No. 2 and No. 4 are the poplar woods (*Populus* spp.), sample No. 3 is the large-fruited elm wood (*Ulmus macrocarpa*), and sample No. 5 is spruce wood (*Picea* sp.). Scientific and accurate identification of wood species provides a guidance and basis for the better analysis of material degradation.

2. The observation of polarization and fluorescence showed that the brightness of crystalline cellulose birefringence in cell walls of the lace-bark pine and spruce wooden components was reduced greatly, demonstrating a large reduction of the cellulose content; whereas that in cell walls of the poplar and elm wooden components was as evident as in the control samples, indicating that the cellulose and lignin compositions remained constant.

3. The analysis of FTIR spectra showed that the absorption peaks representing cellulose and hemicellulose in the lace-bark pine and spruce wooden components disappeared or decreased, whereas those representing the lignin remained constant or showed a large increase, indicating a decrease in the relative content of cellulose and hemicellulose; the absorption peaks in the poplar and elm wooden components, however, remained constant, as in the control samples.

4. From the observations of the polarization and fluorescence effect and the analysis of FTIR spectra, it can be concluded that the lace-bark pine and spruce wooden components were severely attacked by brown rot fungi; in contrast, the poplar and elm wooden components were not attacked by wood decay fungi, but by insects. These results provide scientific guidance for subsequent preventive conservation such as preservative treatment and insect prevention treatment.

Acknowledgments

The authors gratefully acknowledge the financial support from Cross-Science Research Project of Nanyang Institute of Technology (230068) and Scientific Research Start-Up Projects of Nanyang Institute of Technology (510144).

Literature Cited

Bari, E., G. Daniel, N. Yilgor, J. S. Kim, M. A. Tajick-Ghanbary, A. P. Singh, and J. Ribera. 2020. Comparison of the decay behavior of two white-rot fungi in relation to wood type and exposure conditions. *Microorganisms* 8. https://doi.org/10.3390/microorganisms8121931

Bari, E., M. G. Daryaei, M. Karim, M. Bahmani, O. Schmidt, S. Woodward, M. A. T. Ghanbary, and A. Sistani. 2019. Decay of *Carpinus betulus* wood by *Trametes versicolor*—An anatomical and chemical study. *Int. Biodeterior. Biodegradation* 137:68–77. https://doi.org/10.1016/j.ibiod.2018.11.011

Broda, M. and C. M. Popescu. 2019. Natural decay of archaeological oak wood versus artificial degradation processes—An FT-IR spectroscopy and X-ray diffraction study. *Spectrochim. Acta Part A: Mol. Biomol. Spectrosc*. 209:280–287. https://doi.org/10.1016/j.saa.2018.10.057

Broda, M., C. M. Popescu, S. F. Curling, D. I. Timpu, and G. A. Ormondroyd. 2022. Effects of biological and chemical degradation on the properties of scots pine wood—Part i: Chemical composition and microstructure of the cell wall. *Materials* 15:2348. https://doi.org/10.3390/ma15072348

Cheng, J. Q., J. J. Yang, and P. Liu. 1992. Chinese Timber Records. China Forestry Publishing House, Beijing.

Croitoru, C., C. Spirchez, A. Lunguleasa, D. Cristea, I. C. Roata, M. A. Pop, T. Bedo, E. M. Stanciu, and A. Pascu. 2018. Surface properties of thermally treated composite wood panels. *Appl. Surf. Sci*. 438:114–126. https://doi.org/10.1016/j.apsusc.2017.08.193

Diandari, A. F., Djarwanto, L. M. Dewi, and Iriawati. 2020. Anatomical characterization of wood decay patterns in *Hevea brasiliensis* and *Pinus merkusii* caused by white-rot fungi: *Polyporus arcularius* and *Pycnoporus sanguineus*. *IOP Conf. Ser.: Earth Environ. Sci.* 528. https://doi.org/10.1088/1755-1315/528/1/012048

Dong, S. H., C. Wang, J. K. Xiang, and G. Zhang. 2020. Research on changes of chemical composition and structure of the minor carpentry work in Gongshu Hall of Hu County based on FTIR-ATR. *Infrared* 41(7):30–37. https://doi.org/10.3969/j.issn.1672-8785.2020.07.006

Fahey, L. M., M. K. Nieuwoudt, and P. J. Harris. 2019. Predicting the cell-wall compositions of solid *Pinus radiata* (radiata pine) wood using NIR and ATR FTIR spectroscopies. *Cellulose* 26(13–14):7695–7716. https://doi.org/10.1007/s10570-019-02659-8

GB/T16734-1997. 1997. Names of Chinese main woods. State Bureau of Technical Supervision of the People's Republic of China.

GB/T29894-2013. 2013. General method of wood identification. State Quality Supervision, Inspection and Quarantine Administration of the People's Republic of China.

Guo, M. L., H. F. Lan, and J. Qiu. 2010. Wood deterioration and preservation. China Metrology Publishing House, Beijing.

Kanbayashi, T. and H. Miyafuji. 2016. Effect of ionic liquid treatment on the ultrastructural and topochemical features of compression wood in Japanese cedar (*Cryptomeria japonica*). *Sci. Rep.* 6. https://doi.org/10.1038/srep30147

Kiyoto, S., A. Yoshinaga, E. Fernandez-Tendero, A. Day, B. Chabbert, and K. Takabe. 2018. Distribution of lignin, hemicellulose, and arabinogalactan protein in hemp phloem fibers. *Microsc. Soc. Canada* 24(4):442–452. https://doi.org/10.1017/S1431927618012448

Liu, C. W., M. L. Su, X. W. Zhou, R. J. Zhao, J. X. Lu, and Y. R. Wang. 2017. Analysis of content and distribution of lignin in cell wall of transgenic poplar with Fourier infrared spectrun (FTIR) and confocal laser scanning microscopy (CLSM). *Spectrosc. Spectr. Anal*. 37(11):3404–3408. https://doi.org/10.3964/j.issn.1000-0593(2017)11-3404-05

Liu, Y. X. and G. J. Zhao. 2012. Wood Science. China Forestry Publishing House, Beijing.

Richter, H. G., D. Grosser, I. Heinz, and P. E. Gasson. 2004. IAWA list of microscopic features for softwood identification. *IAWA J*. 25(1):1–70. https://doi.org/10.1163/22941932-90000349

Sun, H., Y. Yang, Y. X. Han, M. J. Tian, B. Li, L. Han, A. F. Wang, W. Wang, R. Zhao, and Y. M. He. 2020. X-ray photoelectron spectroscopy analysis of wood degradation in old architecture. *BioResources* 15(3):6332–6343. https://doi.org/10.15376/biores.15.3.6332-6343

Tamburini, D., J. J. Lucejko, B. Pizzo, M. Y. Mohammed, R. Sloggett, and M. P. Colombini. 2017. A critical evaluation of the degradation state of dry archaeological wood from Egypt by SEM, ATR-FTIR, wet chemical analysis and Py(HMDS)-GC-MS. *Polym. Degrad. Stab*. 146:140–154. https://doi.org/10.1016/j.polymdegradstab.2017.10.009

Ueda, R., K. Sawata, R. Takanashi, Y. Sasaki, and T. Sasaki. 2020. Degradation of shear performance of screwed joints caused by wood decay. *J. Wood Sci*. 66(1):1–11. https://doi.org/10.1186/s10086-020-01889-w

Wentzel, M., A. Rolleri, H. Pesenti, and H. Militz. 2019. Chemical analysis and cellulose crystallinity of thermally modified *Eucalyptus nitens* wood from open and closed reactor systems using FTIR and X-ray crystallography. *Eur. J. Wood Wood Prod*. 77(4):517–525. https://doi.org/10.1007/s00107-019-01411-0

Wheeler, E. A., P. Baas, and P. E. Gasson. 1989. IAWA list of microscopic features for hardwood. *IAWA Bull*. 10(3):219–332.

Yang, Y., B. Li, H. Sun, Y. L. Fan, A. F. Wang, R. Zhao, W. Wang, and Y. M. He. 2022c. Study on the decay extent of wooden components of Danxia Temple ancient building by polarized light, fluorescence and

X-ray diffraction methods. *Cellul*. *Chem. Technol*. 56(7–8):717–726. https://doi.org/10.35812/CelluloseChemTechnol.2022.56.63

Yang, Y., H. Sun, B. Li, L. Han, A. F. Wang, W. Wang, Y. M. He, and R. Zhao. 2022a. Study on the identification and the extent of decay of the wooden components in the Xichuan Guild Hall ancient architectures. *Int. J. Archit. Herit*. 16(3):405–414. https://doi.org/10.1080/15583058.2020.1786190

Yang, Y., H. Sun, B. Li, A. F. Wang, R. Zhao, W. Wang, Y. M. He, S. Yang, Y. X. Han, and W. Y. Sun. 2020a. FTIR analysis of the chemical composition changes of wooden components in the ancient architectures of Xichuan Guild Hall. *Forest Prod. J*. 70(4):448–452. https://doi.org/10.13073/FPJ-D-20-00028

Yang, Y., H. Sun, S. Yang, W. Y. Sun, Y. Zhao, B. Li, W. Wang, X. Q. Zhang, S. L. Jiang, and Q. Xu. 2021b. Fourier-transform infrared spectroscopy analysis of the changes in chemical composition of wooden components: Part ii—The ancient building of Danxia Remple. *Forest Prod. J*. 71(3):283–289. https://doi.org/10.13073/FPJ-D-21-00015

Yang, Y., H. Sun, S. Yang, A. Wang, R. Zhao, W. Wang, Y. M. He, B. Li, B. X. Zhang, and Q. Wu. 2021a. Internal cause analysis of damage of wooden components in Danxia Temple ancient architectures: Tree species. *Wood Res*. 66(2):297–308. https://doi.org/10.37763/wr.1336-4561/66.2.297308

Yang, Y., X. Q. Zhang, Q. Xu, P. Y. Wang, S. L. Jiang, Y. Min, W. Y. Sun, B. Li, Y. L. Fan, and S. Yang. 2022b. Evaluation of the decay levels of wooden components in arcade buildings in the ancient town of Chikan via polarized light, fluorescence and FTIR spectra. *Wood Res*. 67(4):545–557. https://doi.org/10.37763/wr.1336-4561/67.4.545557